

## Supporting Information

### Structure reorganization-controlled electron transfer of bipyridine derivatives as organic redox couples

Yang Lv,<sup>a</sup> Yiyang Liu,<sup>a</sup> Ting Feng,<sup>a</sup> Jin Zhang,<sup>a</sup> Shanfu Lu,<sup>a</sup> Haining Wang<sup>\*a,b</sup> and Yan Xiang<sup>\*a</sup>

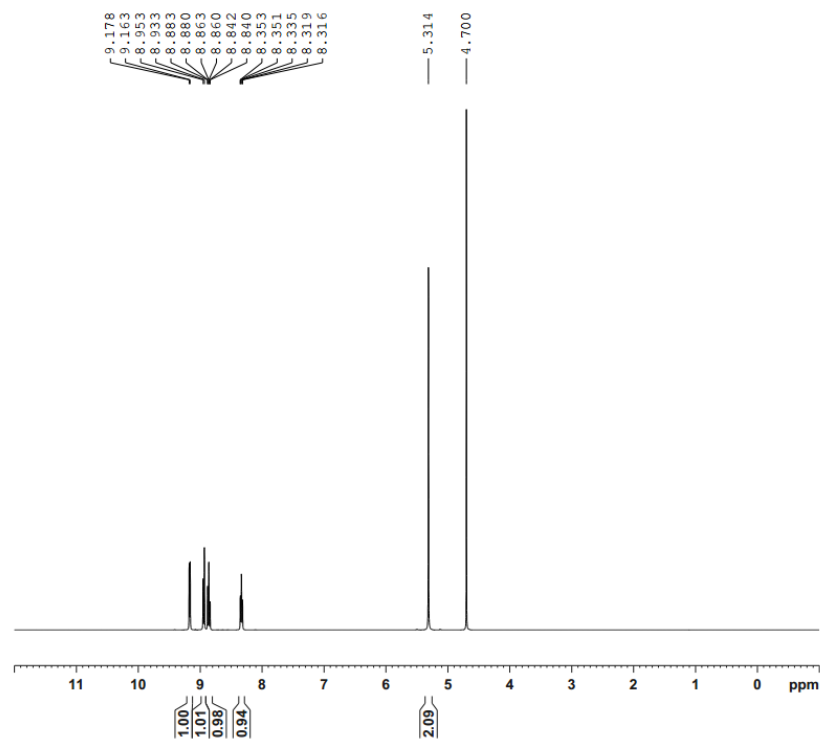
<sup>a</sup>Beijing Key Laboratory of Bio-inspired Energy Materials and Devices, School of Space and Environment, Beihang University, Beijing 100191, P. R. China. E-mail: hwang@buaa.edu.cn; xiangy@buaa.edu.cn

<sup>b</sup>Department of Chemistry, University of Central Florida, Orlando, FL 32816, USA

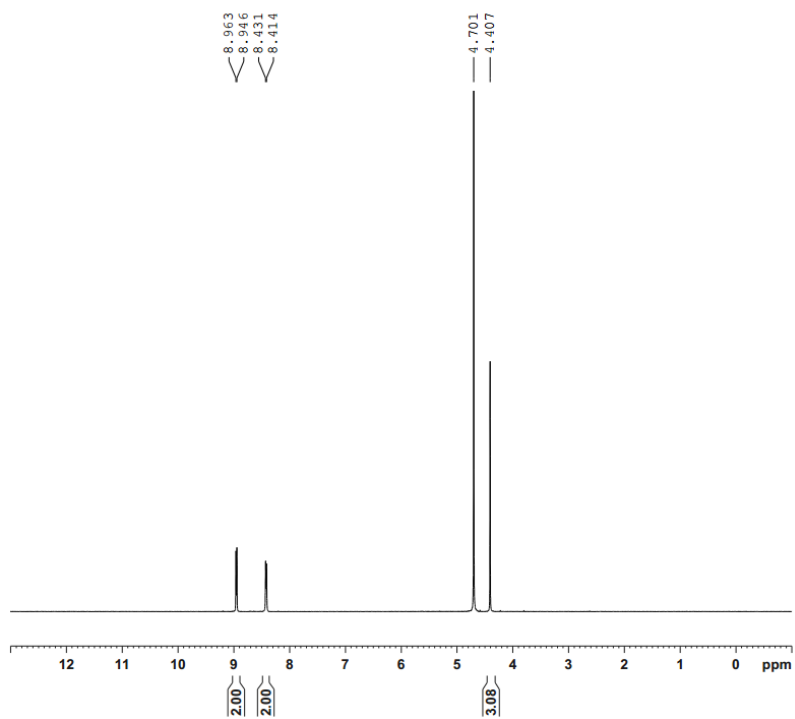
## **Table of Contents**

<b>The <math>^1\text{H-NMR}</math> spectra of DQ<math>^{2+}</math>, MV<math>^{2+}</math> and DM<math>^{2+}</math></b>	<b>3-5</b>
<b>Electrochemical measurement and schematic diagram for reorganization energy theoretical calculation</b>	<b>6-11</b>
<b>Physical property of DQ<math>^{2+}</math>, MV<math>^{2+}</math> and DM<math>^{2+}</math></b>	<b>12</b>
<b>Single cell test</b>	<b>13-18</b>
<b>References</b>	<b>19</b>

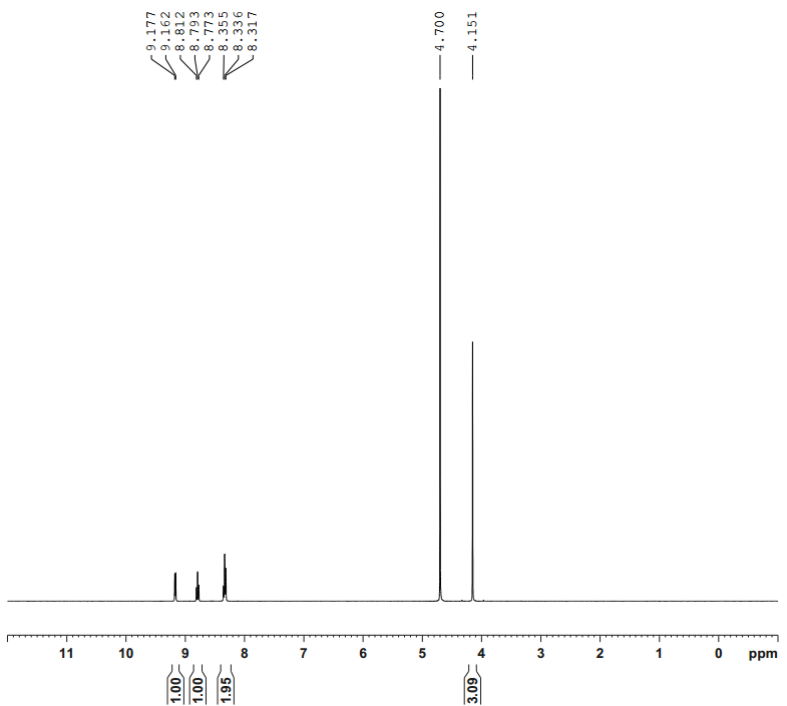
## <sup>1</sup>H-NMR spectra of DQ<sup>2+</sup>, MV<sup>2+</sup> and DM<sup>2+</sup>



**Figure S1.** <sup>1</sup>H NMR spectrum of DQ<sup>2+</sup>. <sup>1</sup>H NMR (400 MHz, D<sub>2</sub>O) δ = 9.17 (d, J=6.0, 2H), 8.94 (d, J=8.0, 2H), 8.86 (td, J=8.1, 1.1, 2H), 8.38 – 8.29 (m, 2H), 5.31 (s, 2H).

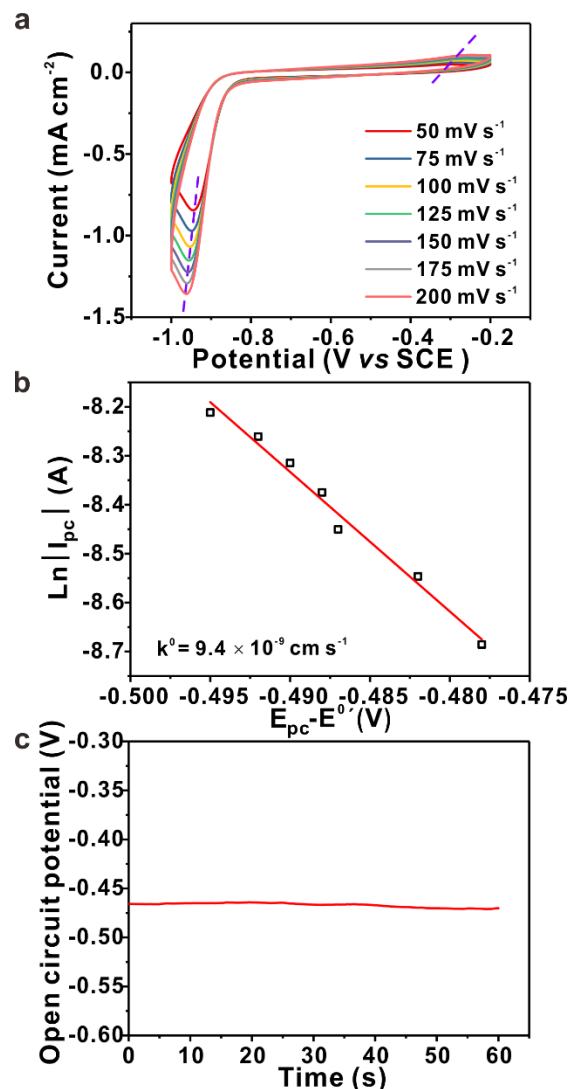


**Figure S2.**  $^1\text{H}$  NMR spectrum of  $\text{MV}^{2+}$ .  $^1\text{H}$  NMR (400 MHz,  $\text{D}_2\text{O}$ )  $\delta$  = 8.95 (d,  $J$ =6.7, 2H), 8.42 (d,  $J$ =6.5, 2H), 4.41 (s, 3H).

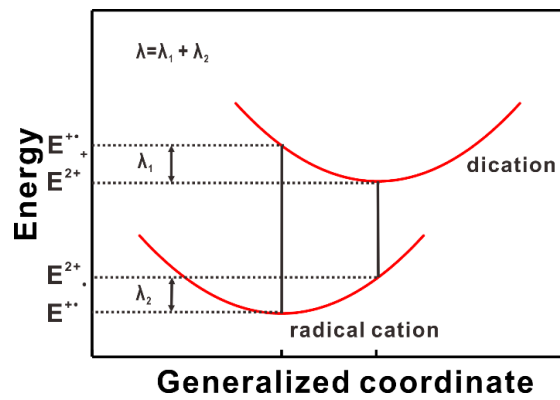


**Figure S3.** <sup>1</sup>H NMR spectrum of DM<sup>2+</sup>. <sup>1</sup>H NMR (400 MHz, D<sub>2</sub>O) δ = 9.17 (d, J=6.0, 2H), 8.79 (t, J=7.9, 2H), 8.34 (t, J=7.7, 4H), 4.15 (s, 6H).

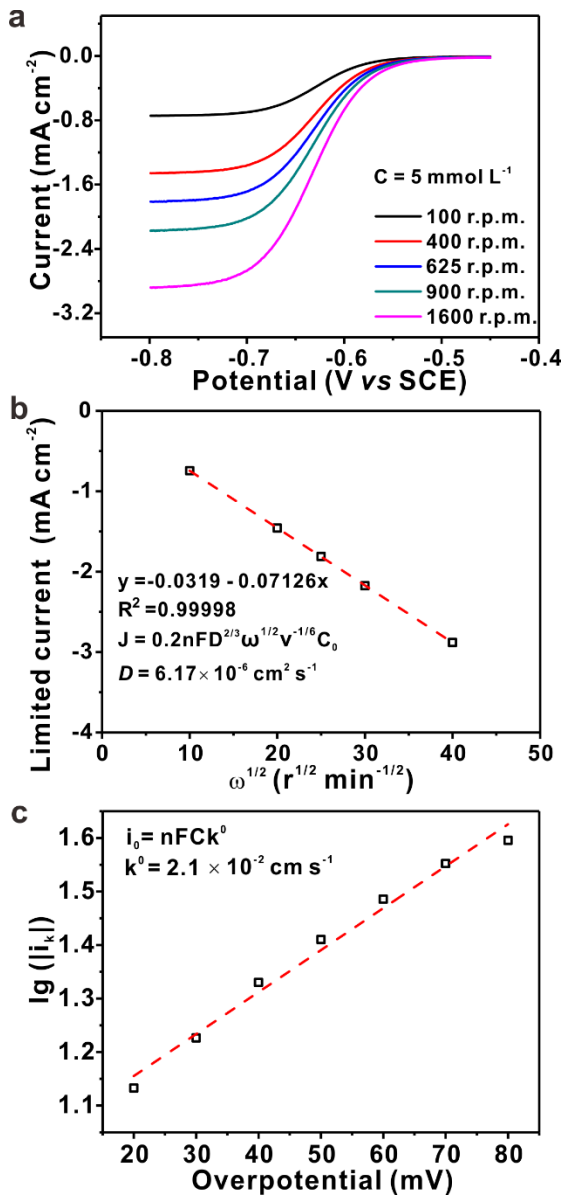
**Electrochemical measurement and schematic diagram for reorganization energy theoretical calculation**



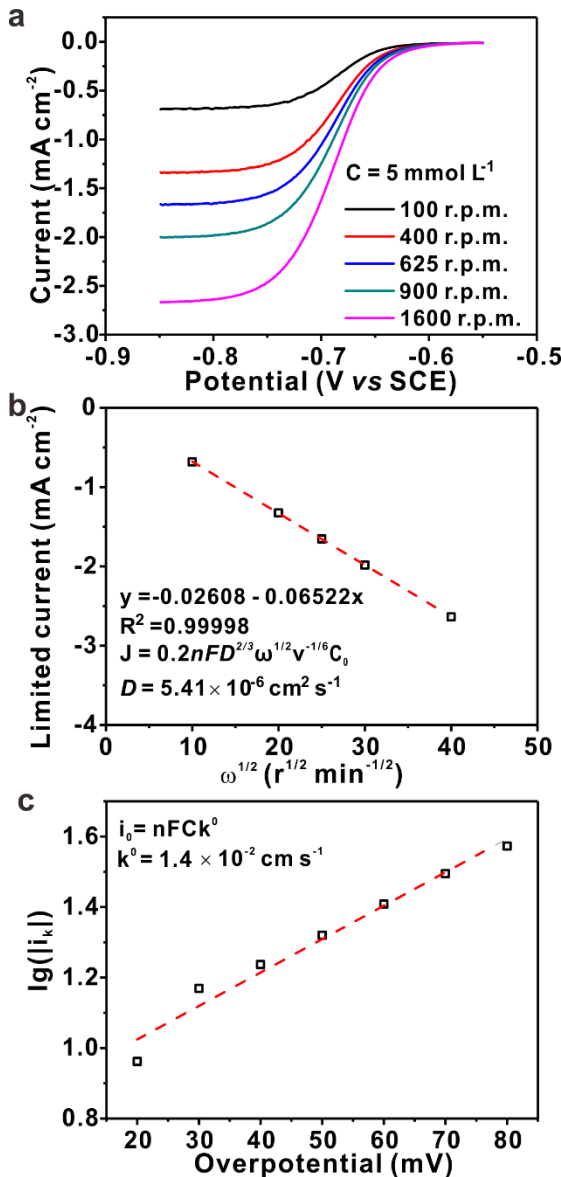
**Figure S4.** (a) The cyclic voltammograms curves of  $5 \text{ mmol L}^{-1}$   $\text{DM}^{2+}$  in  $0.5 \text{ mol L}^{-1}$   $\text{NaCl}$  solution under different scanning rates. (b) The plots of napierian logarithm of cathodic peak current versus the difference between the cathodic potentials and formal potentials for  $\text{DM}^{2+}$ . (c) The open circuit potential of  $\text{DM}^{2+}$  in  $0.5 \text{ mol L}^{-1}$   $\text{NaCl}$  solution (the concentration of  $\text{DM}^{2+}$  and  $\text{DM}^{+•}$  are both  $5 \text{ mmol L}^{-1}$ .)



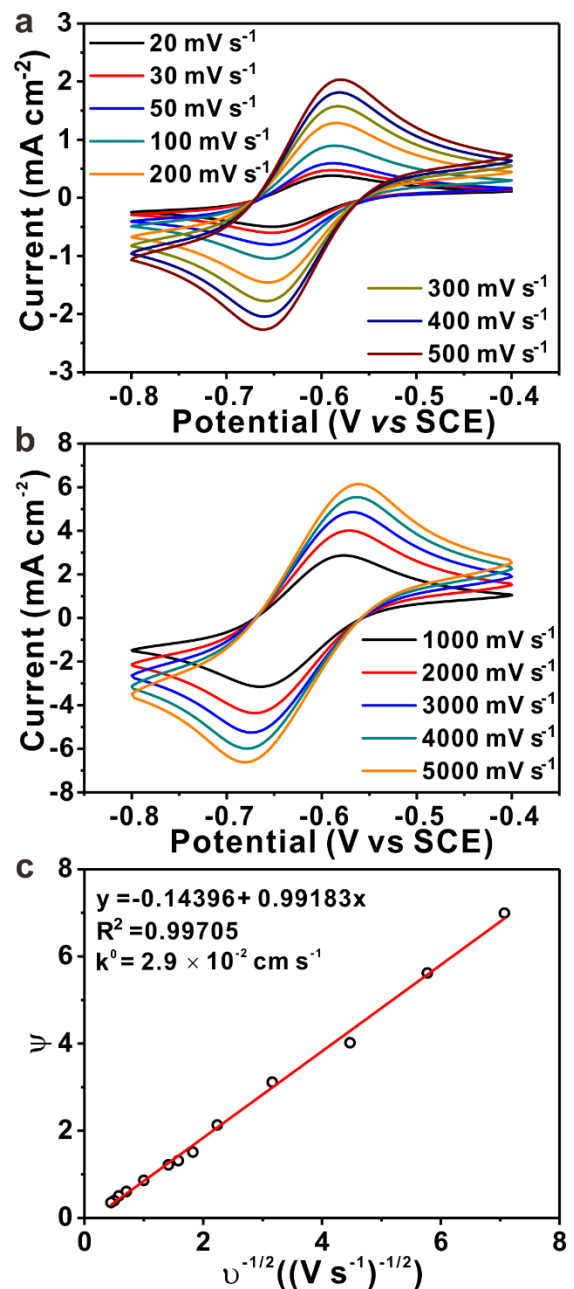
**Figure S5.** The schematic diagram for reorganization energy calculation based on Marcus-Hush theory.  $E^{2+}$  and  $E^{2+}$  are the energy of the radical cation molecule and dication molecule respectively.  $E^{2+\bullet}$  is the energy of the radical cation molecule with the optimized geometry of the dication molecule, and  $E^{2+\bullet+}$  is the energy of the dication molecule with the optimized geometry of the radical cation molecule.



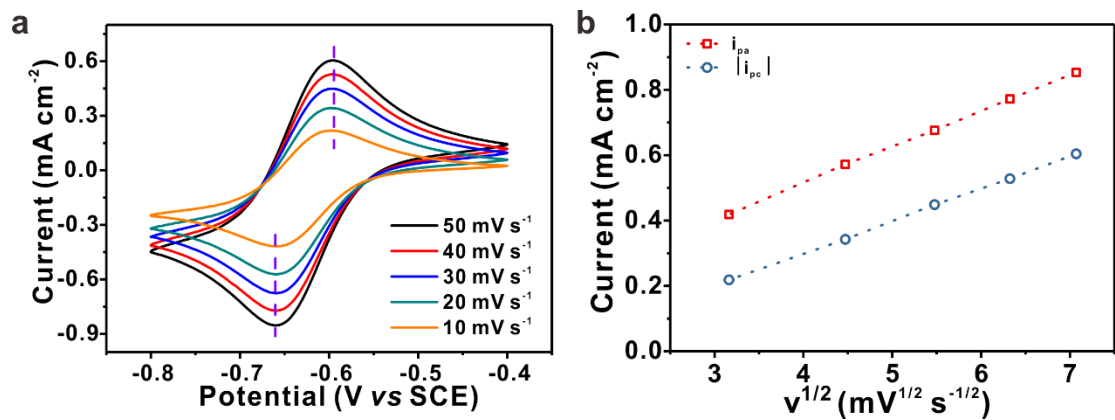
**Figure S6.** (a) The linear sweep voltammograms curves of  $5 \text{ mmol L}^{-1}$   $\text{DQ}^{2+}$  in  $0.5 \text{ mol L}^{-1}$   $\text{NaCl}$  solution with the rotation rates varies from 100 to 1600 rpm. (b) The Levich plots of the limiting currents versus the square root of rotation rates for  $\text{DQ}^{2+}$ . (c) The plots of logarithm of kinetic currents versus the over potentials and the corresponding fitted Tafel plots for  $\text{DQ}^{2+}$ .



**Figure S7.** (a) The linear sweep voltammograms curves of  $5 \text{ mmol L}^{-1} \text{ MV}^{2+}$  in  $0.5 \text{ mol L}^{-1} \text{ NaCl}$  solution with the rotation rates varies from 100 to 1600 rpm. (b) The Levich plots of the limiting currents versus the square root of rotation rates for  $\text{MV}^{2+}$ . (c) The plots of logarithm of kinetic currents versus overpotentials and the corresponding fitted Tafel plots for  $\text{MV}^{2+}$ .

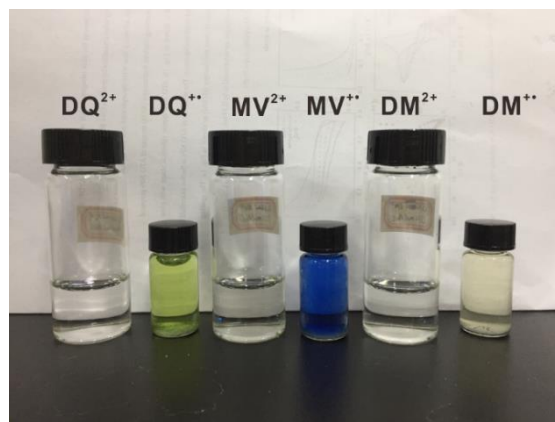


**Figure S8.** (a), (b) Cyclic voltammograms of 5 mmol L<sup>-1</sup> DQ<sup>2+</sup> in 0.5 mol L<sup>-1</sup> NaCl solutions at different scanning rates. (c) Plot of  $\Psi$  vs.  $v^{-1/2}$  toward DQ<sup>2+</sup> (The linear relationship was shown with scan rates of 20 to 5000 mV s<sup>-1</sup>).

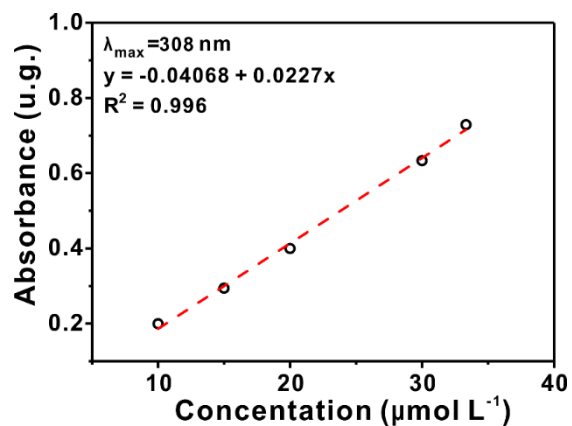


**Figure S9.** (a) The cyclic voltammograms cures of 5 mmol L<sup>-1</sup> DQ<sup>2+</sup> in 0.5 mol L<sup>-1</sup> NaCl solution under different scanning rates. (b) The variation peak currents as a function of the square root of the scan rates of DQ<sup>2+</sup>.

## Physical property of DQ<sup>2+</sup>, MV<sup>2+</sup> and DM<sup>2+</sup>

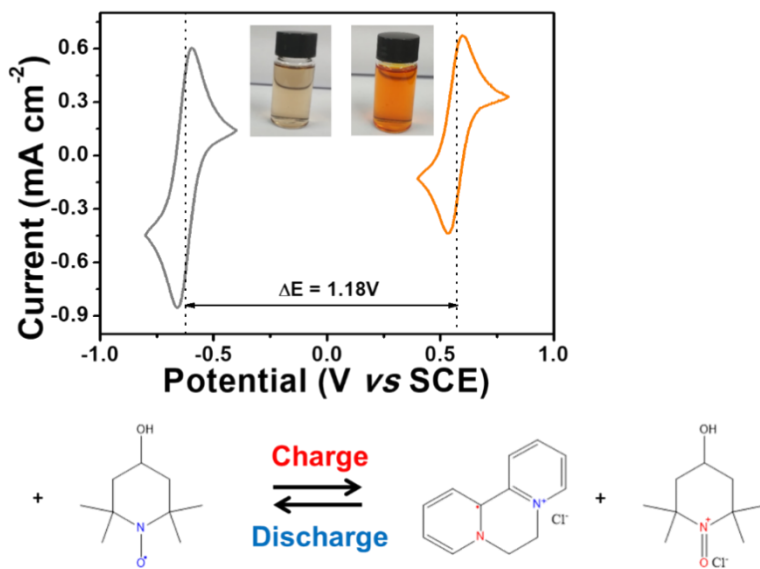


**Figure S10.** The photograph of 0.0325 mmol L<sup>-1</sup> DQ<sup>2+</sup>, MV<sup>2+</sup>, DM<sup>2+</sup> and their monocation radical species.

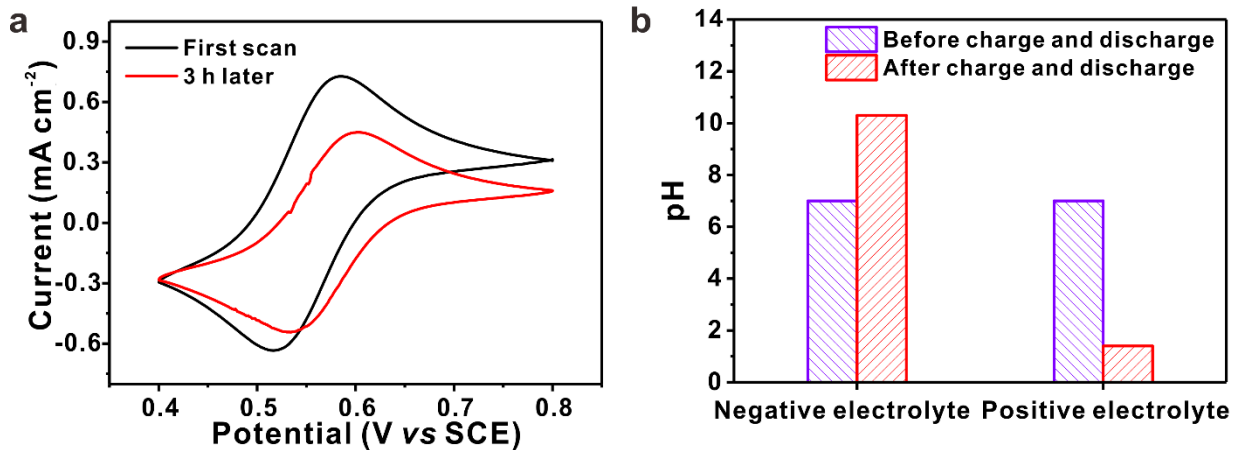


**Figure S11.** The standard curves of DQ<sup>2+</sup> by UV-Vis spectrophotometry measurements.

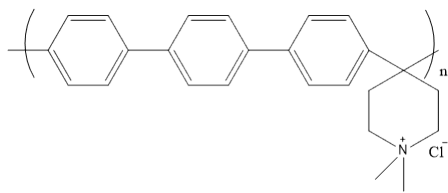
## Single cell test



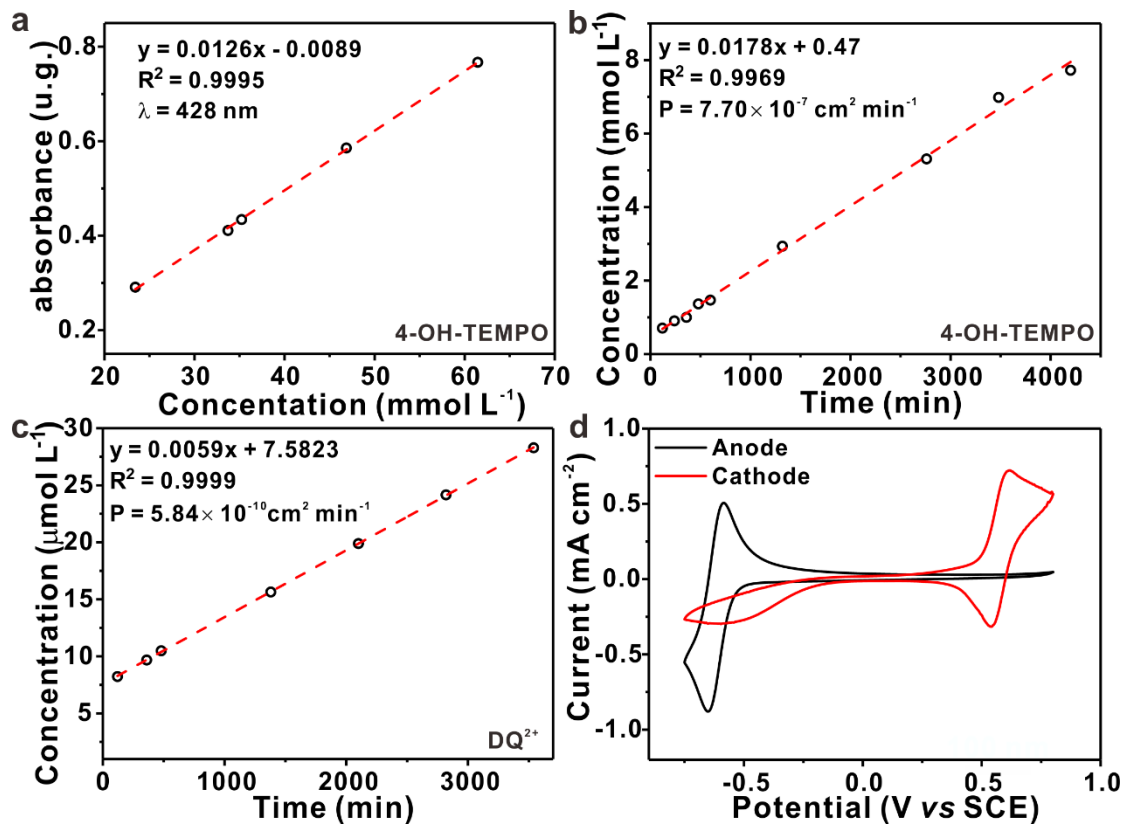
**Figure S12.** A schematic of the  $\text{DQ}^{2+}/4\text{-HO-TEMPO}$  total neutral-aqueous organic redox flow battery.



**Figure S13.** (a) The cyclic voltammograms curves of  $5 \text{ mmol L}^{-1}$  4-OH-TEMPO in  $0.5 \text{ mol L}^{-1}$   $\text{H}_2\text{SO}_4$  solutions. (b) The pH values of electrolyte during 150 cycles (Negative electrolyte:  $0.2 \text{ mol L}^{-1}$   $\text{DQ}^{2+} + 1.0 \text{ mol L}^{-1}$   $\text{NaCl}$ ; Positive electrolyte:  $0.2 \text{ mol L}^{-1}$  4-OH-TEMPO +  $1.0 \text{ mol L}^{-1}$   $\text{NaCl}$ ).

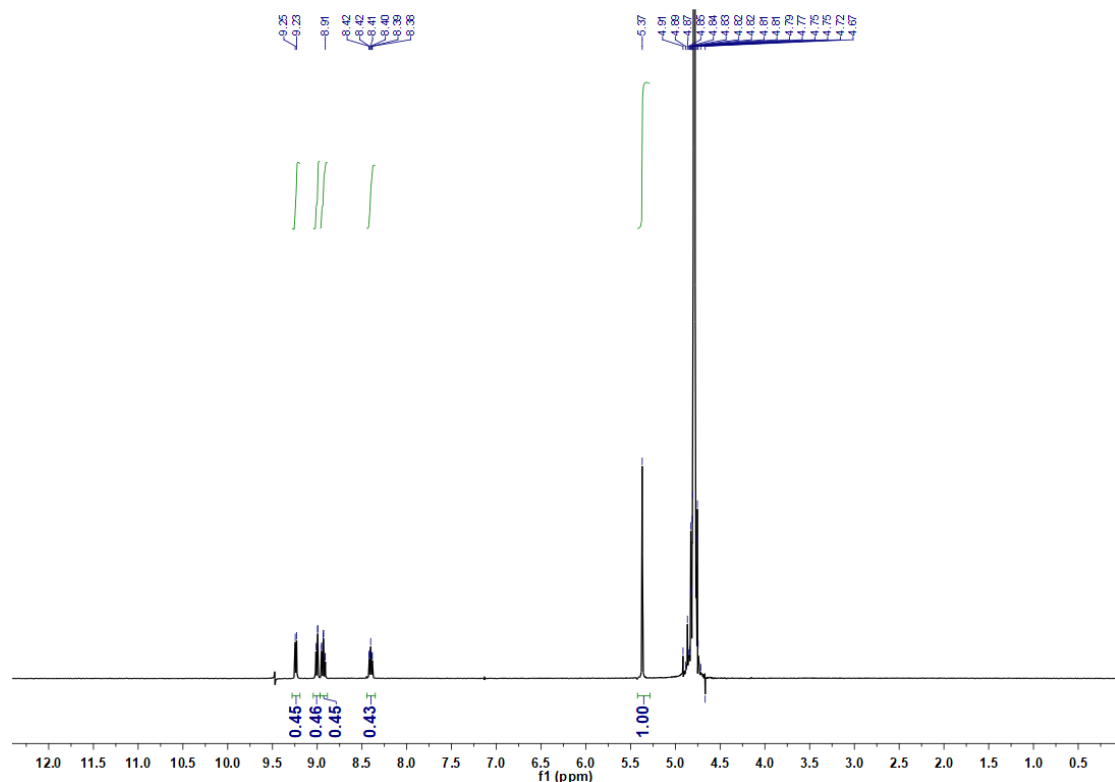


**Figure S14.** The molecular formula of the anion exchange membrane.

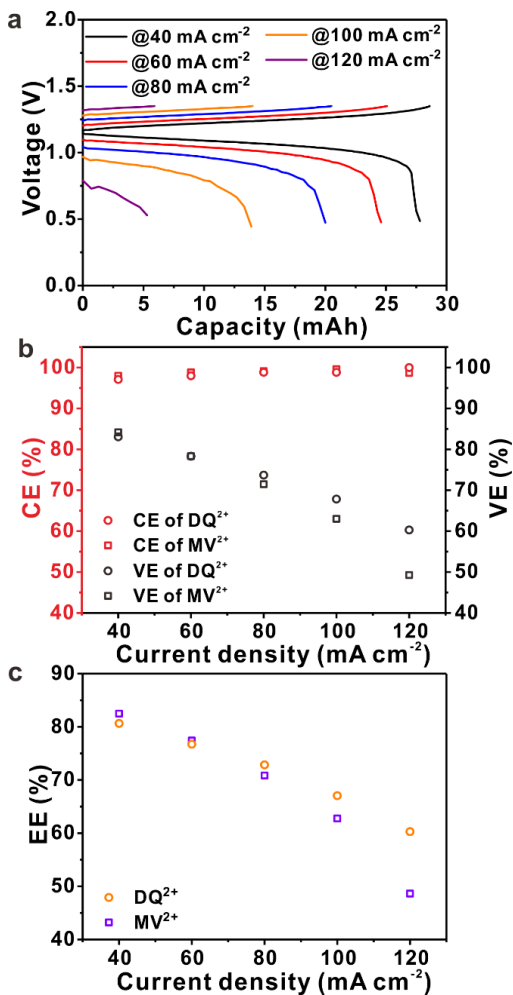


**Figure S15.** (a) The standard curves of 4-OH-TEMPO by UV-Vis spectrophotometry measurements. (b) Concentration of 4-OH-TEMPO in NaCl solution varied with time for QAPPT membrane. (c) Concentration of DQ<sup>2+</sup> in NaCl solution varied with time for QAPPT membrane. (d) Post-cycling CV analysis of anode and cathode solutions after 50 cycles. (Active material in each anode or cathode electrolyte diluted to 5 mmol L<sup>-1</sup>

in 0.5 mol L<sup>-1</sup> NaCl supporting electrolyte, 50 mV s<sup>-1</sup> scan rate, glassy carbon working electrode, glassy carbon counter electrode, saturated calomel reference electrode.)

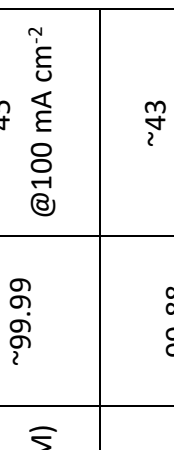
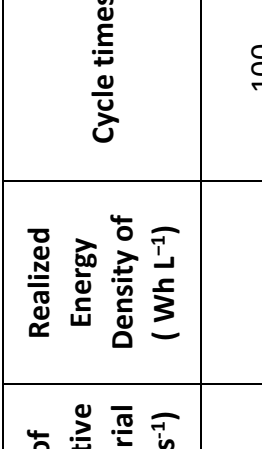
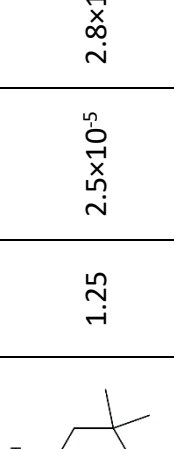
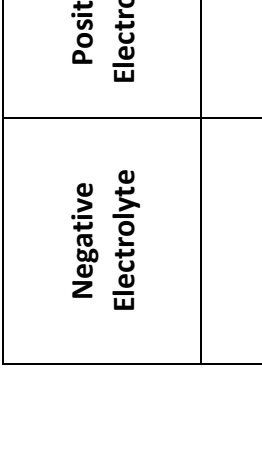


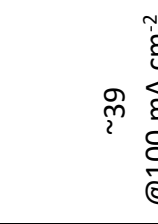
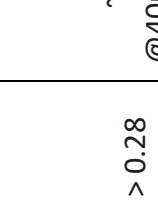
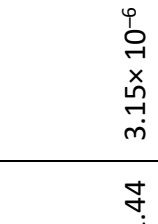
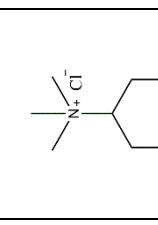
**Figure S16.** Post-cycling <sup>1</sup>H NMR analysis of anode electrolyte after 50 cycles. (50  $\mu$ L electrolyte diluted into 1000  $\mu$ L D<sub>2</sub>O. Residual H<sub>2</sub>O from the electrolyte causes a strong solvent absorption at 4.79 ppm. The signal intensity in anode electrolyte was increased to show no detectable 4-OH-TEMPO within the noise threshold of the instrument. Besides, there is no impurity peak detected in the anode electrolyte, which means DQ<sup>2+</sup> is stable in single cell test.)



**Figure S17.** The cell performance with  $0.2 \text{ mol L}^{-1} \text{MV}^{2+} + 1 \text{ mol L}^{-1} \text{NaCl} + 0.025 \text{ mol L}^{-1} \text{NaH}_2\text{PO}_4$  as negative electrolyte and  $0.2 \text{ mol L}^{-1}$  4-OH-TEMPO +  $1 \text{ mol L}^{-1} \text{NaCl} + 0.025 \text{ mol L}^{-1} \text{NaH}_2\text{PO}_4$  as positive electrolyte (a) The charge and discharge curves for the AORFBs of  $\text{MV}^{2+}$  at different current densities. (b) and (c) The columbic efficiency (CE), voltage efficiency (VE) and energy efficiency (EE) of the AORFBs of  $\text{DQ}^{2+}$  or  $\text{MV}^{2+}$  in different current densities.

**Table S1.** The compare among the viologen derivatives and 2,2'-bypyridine derivatives used in aqueous redox flow battery

Negative Electrolyte	Positive Electrolyte	Volta ge(V)	D of negative material (cm <sup>2</sup> ·s <sup>-1</sup> )	k <sup>0</sup> of negative material (cm·s <sup>-1</sup> )	Realized Energy Density of ( Wh L <sup>-1</sup> )	Cycle times	Capacity Retention /Cycle (%)	Energy efficiency (%)	Ref
		1.25	2.5×10 <sup>-5</sup>	2.8×10 <sup>-4</sup>	~6.4 @40mA cm <sup>-2</sup>	100 (0.1 M/ 0.1 M)	~99.99	~45 @100 mA cm <sup>-2</sup>	1
		1.4	5.7×10 <sup>-6</sup>	3.3×10 <sup>-3</sup>	38 @25mA cm <sup>-2</sup>	100 (0.5 M/ 0.5 M)	99.88	~43 @100 mA cm <sup>-2</sup>	2
		0.75	3.3×10 <sup>-6</sup>	2.2×10 <sup>-2</sup>	13 @25mA cm <sup>-2</sup>	500 (0.75 M/ 1.0 M)	~99.963	~62.5 @100 mA cm <sup>-2</sup>	3
		1	5.4×10 <sup>-6</sup>	>0.36	7.1 @40mA cm <sup>-2</sup>	50 (0.25 M/ 0.5 M)	99.82	45 @100 mA cm <sup>-2</sup>	4

	1.44	$3.15 \times 10^{-6}$	>0.28	$\sim 8.0$ @40mA cm <sup>-2</sup>	50 (0.25 M/ 0.5 M)	99.94	$\sim 39$ @100 mA cm <sup>-2</sup>	5
	KI	1.0	$3.26 \times 10^{-6}$	>0.28	$\sim 6.0$ @60mA cm <sup>-2</sup>	300 (0.5 M/ 2 M)	99.99	$\sim 38$ @100 mA cm <sup>-2</sup>
	KBr	1.49	$5.19 \times 10^{-6}$	>0.36	36.4 @40mA cm <sup>-2</sup>	200 (0.1 M/ 2 M)	N/A	$67.4$ @100 mA cm <sup>-2</sup>
	18	1.89	$3.99 \times 10^{-6}$	>0.31	$\sim 4.4$ @5mA cm <sup>-2</sup>	100 (0.5M/0.5M)	99.8	$\sim 85$ @5 mA cm <sup>-2</sup>
		1.12	$4.6 \times 10^{-6}$	$6.4 \times 10^{-3}$	$\sim 4.4$ @5mA cm <sup>-2</sup>	100 (0.5M/0.5M)	99.8	$\sim 85$ @5 mA cm <sup>-2</sup>
		1.18	$6.2 \times 10^{-6}$	$2.1 \times 10^{-2}$	2.5 @40mA cm <sup>-2</sup>	100 (0.2M/0.2M)	99.95	$67$ @100 mA cm <sup>-2</sup>
								This work

## References

1. T. Liu, X. Wei, Z. Nie, V. Sprenkle and W. Wang, *Adv. Energy Mater.*, 2016, **6**, 1501449.
2. T. Janoschka, N. Martin, M. D. Hager and U. S. Schubert, *Angew. Chem. Int. Ed.*, 2016, **55**, 14427-14430.
3. E. S. Beh, D. De Porcellinis, R. L. Gracia, K. T. Xia, R. G. Gordon and M. J. Aziz, *ACS Energy Lett.*, 2017, **2**, 639-644.
4. C. DeBruler, B. Hu, J. Moss, X. Liu, J. Luo, Y. Sun and T. L. Liu, *Chem*, 2017, **3**, 961-978.
5. J. Luo, B. Hu, C. Debruler and T. L. Liu, *Angew. Chem. Int. Ed.*, 2018, **57**, 231-235.
6. C. DeBruler, B. Hu, J. Moss, J. Luo and T. L. Liu, *ACS Energy Lett.*, 2018, **3**, 663-668.
7. W. Liu, Y. Liu, H. Zhang, C. Xie, L. Shi, Y. G. Zhou and X. Li, *Chem Commun*, 2019, **55**, 4801-4804.
8. J. Huang, Z. Yang, V. Murugesan, E. Walter, A. Hollas, B. Pan, R. S. Assary, I. A. Shkrob, X. Wei and Z. Zhang, *ACS Energy Lett.*, 2018, **3**, 2533-2538.